RESEARCH ARTICLE

Key Points:
- Vegetation removal shows deep soil C loss does increase with thaw, and plant contributions to Reco dilute delta^{13}C signals from deep soil
- Seasonal Reco delta^{13}C suggests warming and permafrost thaw may stimulate deep soil respiration and also surface soil and plant respiration
- Wet conditions may reduce deep soil C loss, with possible effects of altered diffusion dynamics and increased methane cycling on delta^{13}C

Supporting Information:
- Supporting Information S1

Correspondence to:
M. Mauritz,
memauritz@utep.edu

Author Contributions:
Conceptualization: M. Mauritz, E. Pegoraro, V. G. Salmon, M. Taylor, E. A. G. Schuur
Data curation: J. Ledman
Formal analysis: M. Mauritz
Funding acquisition: S. M. Natali, E. A. G. Schuur
Methodology: M. Mauritz, C. Ebert, E. Pegoraro, V. G. Salmon, M. Taylor, E. A. G. Schuur
Resources: E. A. G. Schuur
Supervision: E. A. G. Schuur
Visualization: M. Mauritz
Writing - original draft: M. Mauritz, C. Ebert, E. Pegoraro, M. Taylor
Writing – review & editing: M. Mauritz, G. Celis, C. Ebert, S. M. Natali, E. Pegoraro, V. G. Salmon, C. Schädel, M. Taylor

Using Stable Carbon Isotopes of Seasonal Ecosystem Respiration to Determine Permafrost Carbon Loss

M. Mauritz[1,2] , G. Celis[1] , C. Ebert[1] , J. Hutchings[3] , J. Ledman[1], S. M. Natali[4] , E. Pegoraro[1,5], V. G. Salmon[6] , C. Schädel[1] , M. Taylor[1] , and E. A. G. Schuur[1]

[1]Center for Ecosystem Society and Science (ECOSS), Northern Arizona University, Flagstaff, AZ, USA, [2]Biological Sciences, University of Texas at El Paso, El Paso, TX, USA, [3]Earth and Planetary Sciences, Washington University, St. Louis, MO, USA, [4]Woods Hole Research Center, Falmouth, MA, USA, [5]Department of Biological Sciences, Northern Arizona University, Flagstaff, AZ, USA, [6]Environmental Science Division and Climate Change Science Institute, Oak Ridge National Laboratory, Oak Ridge, TN, USA

Abstract High latitude warming and permafrost thaw will expose vast stores of deep soil organic carbon (SOC) to decomposition. Thaw also changes water movement causing either wetter or drier soil. The fate of deep SOC under different thaw and moisture conditions is unclear. We measured weekly growing-season $\delta^{13}C$ of ecosystem respiration (Reco$\delta^{13}C$) across thaw and moisture conditions (Shallow-Dry; Deep-Dry; Deep-Wet) in a soil warming manipulation. Deep SOC loss was inferred from known $\delta^{13}C$ signatures of plant shoot, root, surface soil, and deep soil respiration. In addition, a 2-year-old vegetation removal treatment (No Veg) was used to isolate surface and deep SOC decomposition contributions to Reco. In No Veg, seasonal Reco$\delta^{13}C$ indicated that deep SOC loss increased as the soil column thawed, while in vegetated areas, root contributions appeared to dominate Reco. The Reco$\delta^{13}C$ differences between Shallow-Dry and Deep-Dry were significant but surprisingly small. This most likely suggests that, under dry conditions, soil warming stimulates root and surface SOC respiration with a negative ^{13}C signature that opposes the more positive ^{13}C signal from increased deep SOC respiration. In Deep-Wet conditions, Reco$\delta^{13}C$ suggests reduced deep SOC loss but could also reflect altered diffusion or methane (CH_4) dynamics. Together, these results demonstrate that frequent Reco$\delta^{13}C$ measurements can detect deep SOC loss and that plants confound the signal. In future studies, soil profile $\delta^{13}C$ measurements, vegetation removal across thaw gradients, and isotopic effects of CH_4 dynamics could further deconvolute deep SOC loss via surface Reco.

Plain Language Summary Carbon (C) stored in permafrost soil is like a global savings account that keeps C out of the atmosphere. Arctic warming makes permafrost soil C vulnerable to microbial decomposition, and C released to the atmosphere would accelerate global warming. In this study we used ^{13}C isotopes, which function like molecular fingerprints, to detect permafrost soil C decomposition from a soil warming experiment that doubled the thawed soil volume and changed soil moisture conditions. We found that permafrost soil C decomposition was best detected when vegetation was removed. Deeper thaw depth had only a small effect on isotopic signatures possibly because the signal from higher permafrost soil C decomposition was overwhelmed by a simultaneous increase in surface soil decomposition and respiration from plants. In wet areas, the isotopic signal changed which could imply reduced permafrost soil C decomposition. In wet areas, methane cycling might also change the isotope signature. We conclude that seasonal ^{13}C sampling could be useful for detecting permafrost soil C decomposition if combined with measurements that can isolate contributions from surface soil, roots, and methane cycling. Developing methods that make it easier to assess permafrost soil C decomposition is critical for estimating the balance of our global C savings account.

1. Introduction

Rising global temperatures are expected to decrease carbon (C) storage in many ecosystems due to increased C losses via soil decomposition and ecosystem respiration (Reco) (Carey et al., 2016; Lloyd & Taylor, 1994; Mahecha et al., 2010). Northern latitudes are particularly vulnerable to C loss because they are warming more rapidly than any other region (IPCC, 2013) and store large amounts soil organic carbon (SOC) in perennially frozen soils (permafrost; Hugelius et al., 2014). Historically, ecosystem productivity has exceeded decomposition in permafrost ecosystems, making them net C sinks. Warming and

permafrost thaw, however, could destabilize permafrost C stocks and cause deep SOC to be released to the atmosphere, shifting the entire region to a net C source (Abbott et al., 2016; Belshe et al., 2013; Dorrepaal et al., 2009; Schuur et al., 2015). The extent to which permafrost ecosystems will become a C source remains uncertain, in part because warming will cause moisture changes due to increased precipitation and because permafrost thaw changes local hydrology. Ice layers in permafrost form an impermeable water barrier that controls flow and drainage patterns across the landscape (Ping et al., 2015). When water from melting ice cannot drain and ice loss causes the ground surface to subside, permafrost thaw creates wetter soil conditions (Jorgenson et al., 2013; O'Donnell et al., 2012; Osterkamp et al., 2009). As thaw progresses, localized subsidence features can expand, causing the landscape to become increasingly wet. On the other hand, cracks in permafrost ice or exposure of gravel layers can lead to drier soils as water drains from the landscape (Liljedahl et al., 2016). Subsidence and increased wetness could be transitional phases during the thaw process, and over the next century, northern permafrost zones are expected to get wetter before they get drier, despite increased precipitation (Lawrence et al., 2015; Watts et al., 2014). Increased soil saturation creates anaerobic soil conditions that limit microbial decomposition rates and could protect SOC from decomposition (Elberling et al., 2013), while drainage is expected to accelerate deep SOC decomposition. Saturated soil conditions shift microbial metabolism toward greater methane (CH_4) production (Olefeldt et al., 2013; Treat et al., 2015). However, even when CH_4 production increases in wet soil conditions, CO_2 flux remains the dominant pathway for C loss (Schädel et al., 2016). Deep permafrost SOC is easily decomposable when it thaws under lab conditions (Schädel et al., 2014). To constrain vulnerability estimates of permafrost ecosystem C, we need a better understanding of how thaw and moisture dynamics affect deep SOC loss in the field (Schuur et al., 2015).

Detecting deep SOC loss in the field is challenging because soil stocks are extremely heterogeneous (Harden et al., 2012; Hicks Pries et al., 2012) and fluxes are small (Lee et al., 2010). Deep SOC respiration during permafrost thaw has been detected with single $Reco\Delta^{14}C$ (Schuur et al., 2009) and dual $Reco\delta^{13}C$ and $Reco\Delta^{14}C$ partitioning (Hicks Pries et al., 2013). However, $\Delta^{14}C$ sample analysis is expensive, and collection is labor-intensive which limits spatial and temporal coverage. Deep SOC loss has also successfully been detected with only $Reco\delta^{13}C$ measurements (Dorrepaal et al., 2009), and the increasing ease of making real-time $\delta^{13}C$ measurements in the field (Midwood & Millard, 2011) could provide a valuable tool for determining permafrost SOC stability. In this study we evaluate the potential of frequent in situ $Reco\delta^{13}C$ measurement to determine how thaw and moisture impact deep SOC loss in a well-studied experimental warming manipulation (CiPEHR). Previous isotopic studies at this site have shown deep SOC loss can increase with only 10 cm deeper thaw (Hicks Pries et al., 2013, 2016; Schuur et al., 2009) but did not evaluate the effects of moisture on deep SOC loss. The $\delta^{13}C$ signatures of individual Reco sources allows the dominant contributions to Reco to be inferred. At the site used for this study, aboveground shoot $\delta^{13}C$ respiration is −22‰, and root respiration is more negative (−25.5‰) because root metabolism relies on depleted lipid compounds (Figure 1a; Bowling et al., 2008, Hicks Pries et al., 2013). Microbial $\delta^{13}C$ respiration from surface soil decomposition (0–25 cm) is −23.5‰ and reflects the mixture of shoot and root litter that contribute to surface SOC formation. With depth, the $\delta^{13}C$ of bulk SOC increases as soil material becomes more decomposed (Schuur et al., 2003) and because SOC at depth is also older and consists of plants that grew in an atmosphere that had fewer fossil fuel emissions and higher atmospheric $\delta^{13}C$ (Suess effect; Ehleringer, 2000, Esmeijer-Liu et al., 2012). Thus, microbial $\delta^{13}C$ respiration increases up to 6‰ from the surface to 80–90-cm depth (Hicks Pries et al., 2013) resulting in an average $\delta^{13}C$ signature of −21.5‰ (25–85 cm; Figure 1a; Hicks Pries et al., 2013, 2016). We sampled $Reco\delta^{13}C$ from the beginning of the growing season until the end of the growing season when plant contributions decline, thaw is deepest, and the ecosystem shifts to a net CO_2 source indicating that respiration dominates the C balance (Figure 1a; Mauritz et al., 2017). Even with isotope partitioning, the strong respiration signal from vegetation can make it difficult to detect deep SOC loss (Nowinski et al., 2010). To further isolate the effects of seasonal thaw on deep SOC contributions, we therefore also measured $Reco\delta^{13}C$ within a plant removal experiment that has been maintained for 2 years and consists only of heterotrophic respiration. We expected that (Figure 1b)

H1. Vegetation removal treatments will show the greatest seasonal $Reco\delta^{13}C$ increase indicating underlying deep SOC respiration when the diluting effect of vegetation is removed.
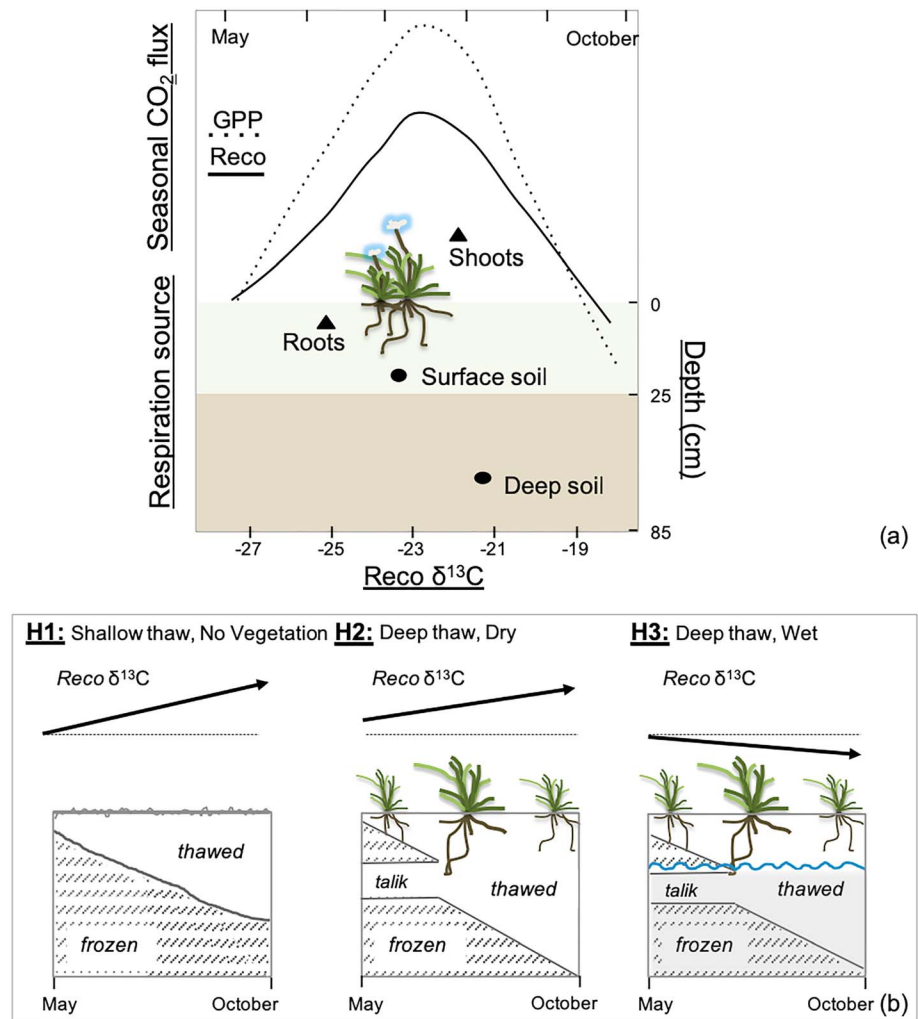
Figure 1. Conceptual figure of growing season gross primary productivity (GPP) and ecosystem respiration (Reco) fluxes from May to October (Mauritz et al., 2017) and average $\delta^{13}C$ respiration signatures from incubations of shoots, roots, surface soil (0-25 cm) and deep soil (25–85 cm; Hicks Pries et al., 2016). (a) Hypothesized seasonal Reco$\delta^{13}C$ patterns (solid arrows) depending on maximum thaw, soil moisture, and plant contributions, relative to Shallow-Dry "reference" (dashed lines). (b) Taliks are persistent, unfrozen soil layers.

H2. In deeply thawed and dry conditions, there will be a stronger seasonal Reco$\delta^{13}C$ increase than in shallow thaw and dry conditions, indicating larger deep SOC loss with thaw.

H3. In deeply thawed and wet conditions, seasonal Reco$\delta^{13}C$ will be lower than in dry areas because saturated soil conditions limit deep SOC loss.

2. Materials and Methods

2.1. Site Description

The site is located in the Eight Mile Lake Watershed, AK, United States (EML; $-149.23°W$, $63.88°N$, 670 m) on a gentle (~3°), northeast-facing slope with well-drained surface soils. The site is underlain by degrading permafrost in the discontinuous permafrost zone (Osterkamp et al., 2009). The site has thick organic horizons (0.25–0.35 m, >20% C) overlaying mineral soils that consist of highly weathered glacial till and loess parent material (5–20% C) and cryoturbated organic inclusions to 1 m (Osterkamp et al., 2009; Pries et al., 2012). The total SOC to 1-m depth is 72 kg/m^2 (Plaza et al., 2017). Throughout the profile, soils are very acidic (pH 3–5), which is typical of Moist Acidic Tundra (Bracho et al., 2016; Osterkamp et al., 2009). Regional long-term mean annual air temperatures were -0.94 °C with summer (May–

September) mean of 11.91 °C and nonsummer (October–April) mean: −10.09 °C (1977–2015 means; Healy and McKinley Stations, Western Regional Climate Center, and National Oceanic and Atmospheric Administration National Centers for Environmental Information [NOAA]). In 2015, the year of study, the summer mean air temperature was 9.53 °C, and nonsummer mean was −8.15 °C (winter 2014/2015). The vegetation is typical of Moist Acidic Tundra, dominated by the tussock-forming sedge *Eriophorum vaginatum*; the shrubs *Betula nana*, *Vaccinium uliginosum*, and *Vaccinum vitis-ideae*; and mosses *Sphagnum spp.*, *Dicranum spp*, and *Pleurozium spp.* (Deane-Coe et al., 2015; Natali et al., 2012; Schuur et al., 2007).

2.2. Experimental Design
2.2.1. Warming and Moisture Manipulation
The Carbon in Permafrost Experimental Heating and Drying Research (CiPEHR and DryPEHR) manipulation was designed to simulate the effect of warmer air and soil temperatures, permafrost degradation, and altered water table on ecosystem C exchange. The experiment is arrayed in three blocks within 100 m of each other in similar landscape positions, with two replicate snow fences per block and seven plots (0.6 m × 0.6 m) per snow fence. Briefly, air warming was achieved using polycarbonate open top chambers (cubicle open top chambers: 0.36 m^2 × 0.5 m), and soil warming was achieved using snow fences that trap snow down-wind and insulate the ecosystem in the winter. Each spring excess snowpack is manually removed to match the ambient snowpack and avoid artifacts such as increased water input and delayed phenology (Walker et al., 1999). The water-table manipulation (DryPEHR) is located within the snow-fence footprint with metal sheets extending 0.6 m into the ground around an intact 2.5 m × 1.5 m tundra area and pumps to remove water. For details on CiPEHR and DryPEHR, see Natali et al. (2011) and Natali et al. (2015), respectively. When CiPEHR was installed in 2008, maximum seasonal extent of permafrost thaw (active layer thickness [ALT]) was approximately 50 cm and has since increased at a rate of 2 cm/year in control areas and 6 cm/year in soil warming areas (Mauritz et al., 2017). Air warming effects are small (0.4 °C) and affected vegetation and CO$_2$ fluxes only in the first year of warming (Mauritz et al., 2017; Natali et al., 2012) and had no effect on leaf tissue δ^{13}C (Salmon et al., 2016) or plant Recoδ^{13}C (Hicks Pries et al., 2016). Since DryPEHR was first installed, the water table manipulation has not been able to overcome the effects of heterogeneous thaw on water movement, and the original treatment assignments no longer describe plot conditions. We have therefore reclassified plots along a continuum of ALT and water table depth (WTD; see section 2.2.3). Measurements from CiPEHR and DryPEHR will be collectively referred to as CiPEHR.

2.2.2. Vegetation Removal
Vegetation removal plots (No Veg: $n = 6$) were established in July 2012 paired with vegetated plots (Veg: $n = 6$), 500 m upslope of CiPEHR with no influence from the warming manipulation. No Veg plots were 0.6 × 0.6 m and trenched to 30 cm to exclude roots. All vascular and nonvascular vegetation were clipped at the surface in July 2011, and vegetation removal plots have been maintained by monthly summer weeding, with very little resprouting or photosynthetic moss tissue observed. Paired plots from the vegetation removal will be collectively referred to as "Veg/No Veg."

2.2.3. Plot Grouping Based on ALT and WTD
Over time, heterogeneous thaw has altered the microtopography in CiPEHR, and plots were classified into three discrete groups depending on ALT and WTD: Shallow-Dry ($n = 19$), Deep-Dry ($n = 9$), and Deep-Wet ($n = 12$; (Figures 2 and S1 in supporting information). The ALT clusters largely matched the soil warming treatment with Shallow plots (<80 cm) located mainly within control and Deep plots (>80 cm) within soil warming sides of the snow fences. Wet and Dry plots were separated based on mean seasonal WTD of −5 cm. Wet plots occurred on both sides of the fence, although they were more often associated with the soil warming treatment. The Veg/No Veg plots could not be classified according to ALT and WTD because there were no WTD measurements. Veg plots had shallow ALT (Figure 2a), and based on landscape position and weekly observations, the WTD was likely very similar to Shallow-Dry groups. We have kept Veg plots distinct from Shallow-Dry because they fall entirely outside the experimental manipulation and represent a gradient in vegetation because they have lower Normalized Difference Vegetation Index (NDVI) compared to Shallow-Dry (Figure 2c). The No Veg plots had shallow ALT, most were well drained (4/6), and some had WTD that fluctuated at or just below the surface (2/5).
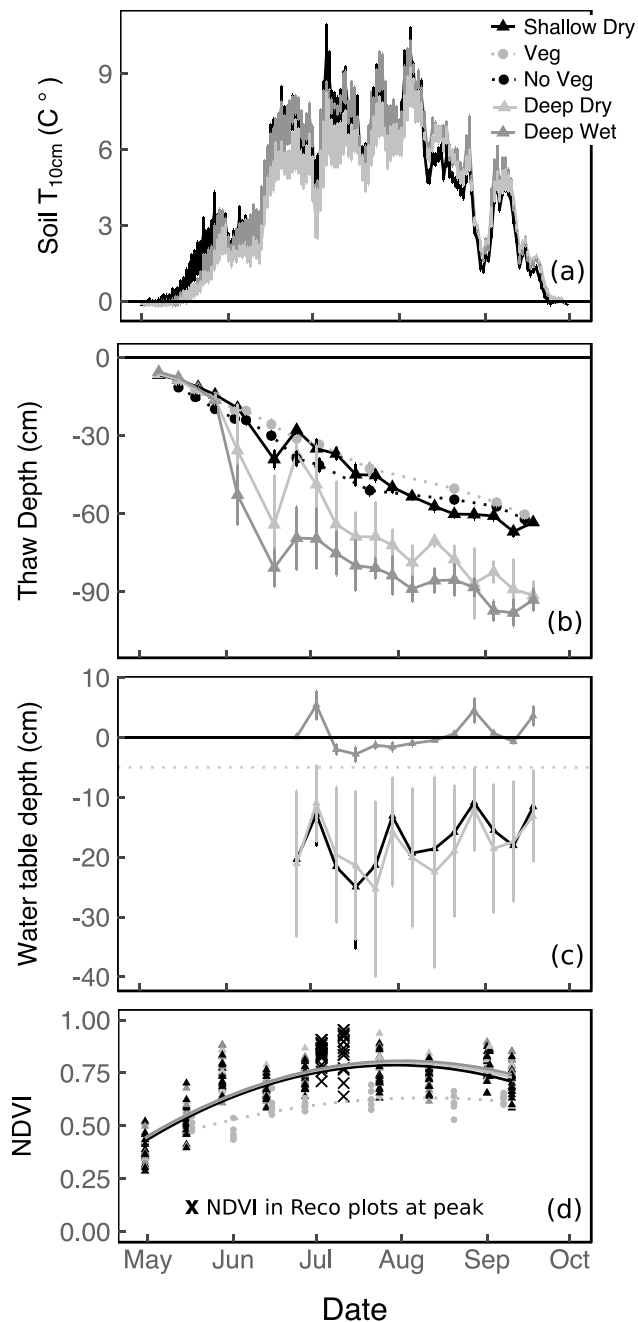
Figure 2. Daily soil temperature at 10-cm depth (a), weekly thaw depth, (b) water table depth from mid-June when wells were ice free (c), and NDVI (d) for all groups in which data were collected. In (c), the horizontal solid line at 0 cm represents the soil surface, and the dotted line at −5 cm marks the water table depth distinction between Wet and Dry groups. Water table was not measured in Veg/No Veg, and No Veg did not have any photosynthetic tissue. In (d), the seasonal NDVI pattern in Carbon in Permafrost Experimental Heating Research comes from paired plots, and "x" show peak NDVI for the Recoδ^{13}C measurement plots. Small error bars for thaw depth in Shallow-Dry, Veg, and No Veg (b) and water table depth in Deep-Wet (c) indicate consistent conditions among plots within those groups. NDVI = Normalized Difference Vegetation Index.

2.3. Environmental Variables and Vegetation Measurements

At CiPEHR, environmental variables and vegetation were measured in paired plots immediately adjacent to each Recoδ^{13}C sampling plot (described below). At Veg/No Veg, all data were collected within Recoδ^{13}C sampling plots. At CiPEHR, soil temperatures were measured half-hourly at 5-, 10-, 20-, and 40-cm depth using type T copper-constantan thermocouples. WTD was measured twice a week within the CiPEHR footprint as in Vogel et al. (2009). WTD was assigned to each plot based on proximity to WTD wells because WTD was not measured within each plot. Thaw depth was measured weekly at both CiPEHR and Veg/No Veg; thaw depth in mid-September (week 36) is close to maximum thaw and was designated as the ALT.

To obtain a metric of seasonal and plot-level differences in biomass and plant activity plot level, NDVI photos were taken using a handheld camera (ADC, Tetracam, CA, United States) at breast height, parallel to the ground. NDVI images were taken on dry and clear days to avoid reflections and diffraction of incoming radiation. Plot-integrated NDVI was calculated from each photo and calibrated to a white Teflon reference tile (PixelWrench2 v 1.2.1.6, Tetracam, CA, United States). At CiPEHR, NDVI was measured weekly in paired plots throughout the season (May–September) and at peak biomass (first week of July) on the Recoδ^{13}C plots. In Veg, NDVI was measured weekly on Recoδ^{13}C sampling plots. The NDVI record ended in early September when frequent rain made it impossible to continue sampling. There are no NDVI measurements for No Veg because there was no green tissue. Further details of environmental and vegetation sampling are in Table S1.

2.4. Ecosystem Respiration and Isotope Measurements
2.4.1. Sampling Frequency
Weekly Reco and Recoδ^{13}C data were collected in 2015 from 15 May to 24 September on a subset of CiPEHR plots at one block (Shallow-Dry: $n = 6$; Deep-Dry: $n = 3$; Deep-Wet: $n = 5$) and at all Veg/No Veg plots ($n = 6$ each). At the peak of the summer growing season, between 9 and 11 July, Reco and Recoδ^{13}C were sampled once across all three CiPEHR blocks to put the temporal trends in greater spatial context (Shallow-Dry: $n = 19$; Deep-Dry: $n = 9$; Deep-Wet: $n = 12$). Measurements were made between 9 am and 6 pm with fully randomized plot sampling order to avoid systematic diurnal bias.

2.4.2. Field Sampling Method
Ecosystem respiration and Recoδ^{13}C were collected using 13-cm-high dark-closed chambers with a coiled vent tube (25 cm long, 0.32 cm inner diameter) to allow pressure equilibration. Chambers fitted onto polyvinyl chloride (PVC) collars (25.4 cm diameter, 10 cm tall, installed 6–7 cm into the organic layer), enclosed intact aboveground vegetation, and created a total sampling volume of 10 L. Collars were installed at CiPEHR in 2008, at DryPEHR in 2011, and Ambient in 2014 and are identical to chambers used previously in manual sampling for Recoδ^{13}C at this site (Hicks Pries et al., 2013, 2016). For each measurement, the chamber was sealed onto the collar, and the headspace was sampled through a cavity ring-down spectrometer (CRDS; G2101i, Picarro Inc., Santa Clara, CA, United States) to measure CO_2 ppm concentrations and δ^{13}C. Air from the chamber was drawn through magnesium perchlorate into the CRDS at a flow-rate of 35 ml/min, sampling frequency of 1.7 s, and total measurement
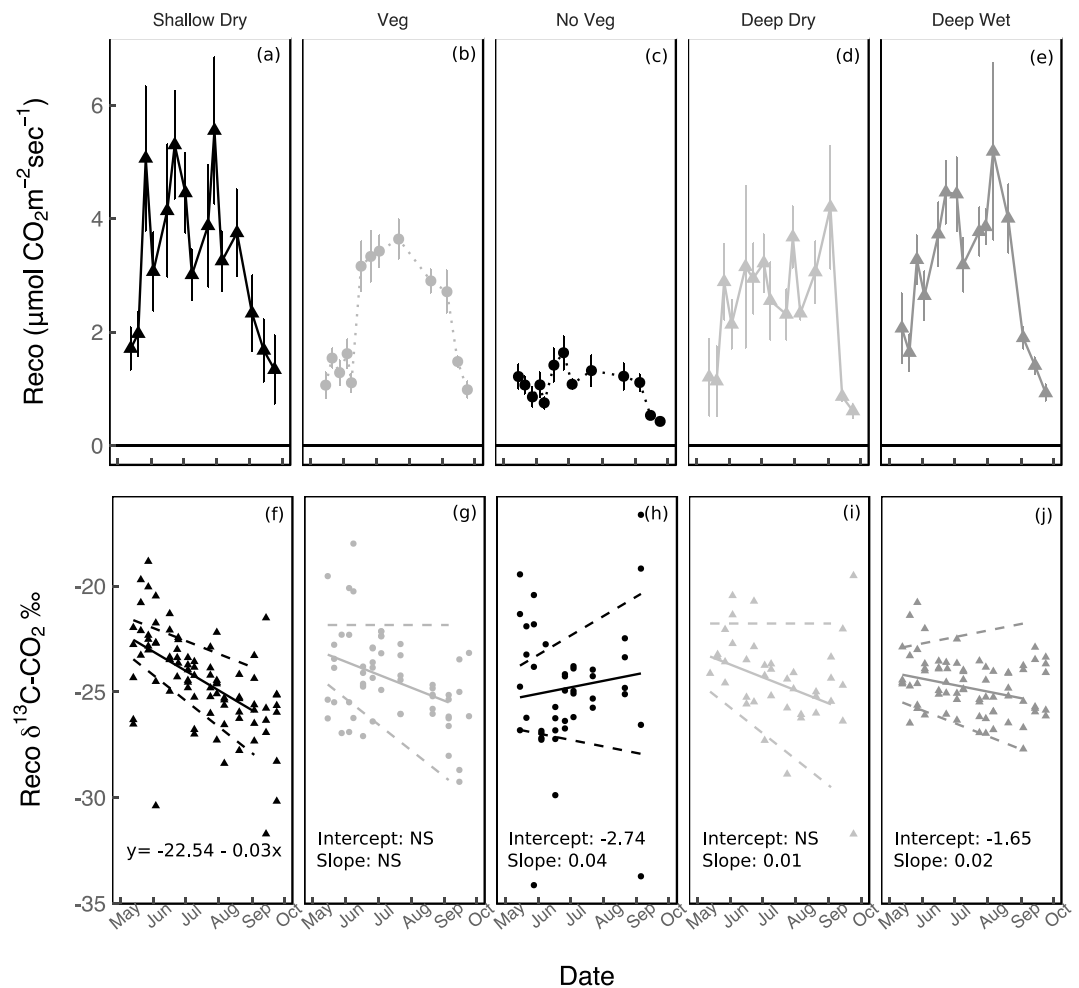
Figure 3. Seasonal Reco flux rates (μmol $CO_2 \cdot m^{-2} \cdot s^{-1}$; a–e) and Reco$\delta^{13}C$ (‰; f–j) in each group. For Reco flux rates, the lines connect mean flux rates (large symbols) on each day of measurement, and error bars represent standard error of the daily mean. For Reco$\delta^{13}C$, the lines are group-specific regression lines and confidence intervals based on the group * time model (Table 2). The equation in (f) shows the Reco$\delta^{13}C$ intercept and slope for Shallow-Dry. In (g)–(j), the effect size of changes in intercept and slope are given for each group. NS indicates no significant difference from Shallow-Dry. For Reco flux rates, significant differences between groups and over time are shown in Table 1.

duration of 15 min. Between each Reco measurement, the sample tubing and CRDS cavity were flushed with atmospheric air for 4 min.

2.4.3. Calculation of Ecosystem Respiration $\delta^{13}C$

Ecosystem respiration $\delta^{13}C$ was determined using Keeling plots where the *y* intercept of a linear regression between $1/[CO_2]$ and $\delta^{13}C$ represents Reco$\delta^{13}C$ (Keeling, 1958, 1961). For each chamber measurement, the periods that represent CO_2 accumulation were selected (Figures S2, S3, and S4a), and raw CO_2 (ppm) and $\delta^{13}C$ measurements were averaged into 30 increment bins (~50 s per bin) to reduce variation associated with the raw $\delta^{13}C$ signal (Figure S4a). Keeling plot intercepts were calculated using Model I ordinary least squares (OLS) regression because Model II reduced major axis produces an incorrect bias toward negative intercepts (Figures S5 and S6; Wehr & Saleska, 2017; Zobitz et al., 2006). Model I OLS has negligible bias at CO_2 ranges greater than 10 ppm (Wehr & Saleska, 2017; our smallest range was 20 ppm) and is the same method previously used at EML (Hicks Pries et al., 2013).

Static chambers can produce nonlinearities in Keeling plots due to altered diffusivity gradients of $^{12}CO_2$ and $^{13}CO_2$ (dynamic fractionation) that arise under nonsteady state conditions. We evaluated the linearity of the

Keeling plots by comparing linear and quadratic fits and found that quadratic coefficients were close to zero and rarely improved the line fit (Figures S4b and 4c). In addition, nonlinearities and biased $Reco\delta^{13}C$ estimates are the smallest during short measurements (<20 min; Nickerson & Risk, 2009a) and decline as chamber height and diameter increase (Ohlsson, 2009). Biases due to nonlinearity can be modeled (Nickerson & Risk, 2009b; Phillips et al., 2010), but we do not attempt to directly quantify diffusivity effects on $Reco\delta^{13}C$ because we have insufficient data about diffusivity and the diffusivity coefficients may themselves be the largest source of error for estimating CO_2 fluxes at this site (Lee et al., 2010). Additionally, it is unclear whether predictions from diffusion models capture sufficient soil complexity to adequately predict or correct $Reco\delta^{13}C$ under field conditions (Snell et al., 2014). Instead, we include interpretations that acknowledge both biological and physical explanations for changes in $Reco\delta^{13}C$.

After calculating Keeling plot intercepts, the $Reco\delta^{13}C$ data were filtered to remove Keeling plots with $R^2 < 0.7$ and less than 5 min of data (Figures S7 and S8). The intercept ($Reco\delta^{13}C$) standard error increased at low CO_2 ranges (Figure S9), which is an unavoidable feature of Keeling plots (Pataki et al., 2003; Wehr & Saleska, 2017; Zobitz et al., 2006). Our R^2 and time-based filtering criteria eliminated $Reco\delta^{13}C$ with intercept standard error > 5‰ (Figures S7 and S9). Filtering criteria for $Reco\delta^{13}C$ (Text S1) removed one No Veg plot all season so that No Veg ($n = 5$).

The Picarro G2101i does not have a user-implemented calibration procedure, so we took repeated samples from a standard CO_2 gas tank to mimic our field sampling technique and applied a postprocessing correction by benchmarking atmospheric $\delta^{13}CO_2$ values at CiPEHR against those measured in Barrow, AK (NOAA Earth System Research Laboratory, https://www.esrl.noaa.gov/gmd/dv/data/). Replicate standard checks for $\delta^{13}C$ were within 1‰ of each other, similar to the external precision of 1–2‰ reported by Midwood and Millard (2011), with a standard deviation of 0.264‰ around the mean of the repeated samples (Figure S10a). The validity of benchmarking CiPEHR atmospheric $\delta^{13}C$ against records in Utqiagvik, AK (formerly Barrow), was based on the similarity in atmospheric $\Delta^{14}C$ at CiPEHR and Utqiagvik which indicates that it is reasonable to assume the air masses are comparable (Text S2; Ebert et al., 2016; Graven et al., 2013; Newman et al., 2016). The regression equation between atmospheric CO_2 and $\delta^{13}C$ in Utqiagvik was used to calculate the expected daily atmospheric $\delta^{13}C$ from CO_2 concentrations at CiPEHR. The difference between expected and measured $\delta^{13}C$ was used to correct instrument offset and potential drift over the season (Text S2 and Figures S11 and S12). For more details on filtering, corrections, and repeated sampling evaluation, see Text S1 and S2 and Figures S5–S13) and code provided with archived data (Mauritz & Schuur, 2018).

2.4.4. Ecosystem Respiration Flux Rate

Ecosystem respiration rates were calculated from raw CO_2 measurements using Model I OLS regression over the same period used to calculate $Reco\delta^{13}C$; all CO_2 fluxes had $R^2 > 0.875$ (Figure S14). Flux rates were converted from concentration to mass by applying the ideal gas law with plot-specific chamber volumes and air temperature and atmospheric pressure at the time of measurement from a meteorological tower at CiPEHR (Natali et al., 2011, 2014). Ecosystem respiration is reported in $\mu mol\ CO_2 \cdot m^{-2} \cdot s^{-1}$.

2.5. Statistics

Seasonal trends were analyzed with linear-mixed effects models. For $Reco\delta^{13}C$, seasonal trends were analyzed with date as a continuous predictor (time) to compare seasonal trends between groups ($Reco\delta^{13}C \sim f$ (group * time)). Shallow-Dry was the reference, and plot and day-of-year (a categorical date variable) were included as random effects to account for plot-level repeated measures and day-to-day deviation from the time trend. Seasonal trends in Reco flux rates were analyzed with a categorical date to better capture the rising and falling seasonal dynamics (Reco ~ f (group * date)). Peak season variation of $Reco\delta^{13}C$ between groups was analyzed by analysis of variance (ANOVA) because each plot was sampled only once during peak.

Normality of all variables was determined by visual inspection of data and model residuals, and data were log transformed when necessary to satisfy normality assumptions. Fixed effects were considered significant if the bootstrapped 95% confidence intervals (CI) did not span zero. Model intercepts, effect sizes, and CI are reported in the units of the dependent variable with the exception of Reco flux rates which were analyzed on a log scale, so we report the model coefficients as percent change.

The best models were selected using stepwise selection in which individual variables were removed and compared to the full model using Akaike Information Criterion adjusted for small sample size (AICc).

Table 1
Seasonal Reco Flux Rate Coefficients for All Groups

Variable	Coefficient	2.5% CI	97.5% CI
Intercept (Shallow-Dry, 13 May)	1.74	1.30	2.35
Veg	−22.28	−45.01	9.64
No Veg	**−62.73**	**−73.93**	**−47.10**
Deep-Dry	−27.84	−52.82	9.12
Deep-Wet	−1.12	−30.91	42.64
20 May	4.53	−17.99	32.74
27 May	**56.14**	**22.95**	**98.67**
3 June	**39.07**	**9.11**	**76.58**
16 June	**107.56**	**62.84**	**163.06**
23 June	**138.72**	**88.14**	**202.69**
3 July	**128.70**	**78.27**	**192.48**
24 July	**115.44**	**67.28**	**176.28**
20 August	**110.26**	**66.61**	**164.54**
3 September	**51.14**	**18.85**	**90.52**
14 September	**−23.24**	**−39.25**	**−3.17**
24 September	**−45.08**	**−58.02**	**−28.69**

Note. The Intercept represents Shallow-Dry on the first sample date, 13 May, in μmol $CO_2 \cdot m^{-2} \cdot s^{-1}$, and the effect of groups or days is reported as a percent change, relative to the intercept. Bold values indicate statistical significance. CI = confidence interval.

Table 2
Seasonal Trend for Recoδ13C

Variable	Coefficient	2.5% CI	97.5% CI
Intercept (Shallow-Dry)	−22.54	−23.46	−21.61
Veg	−0.66	−2.04	0.70
No Veg	**−2.74**	**−4.25**	**−1.28**
Deep-Dry	−0.79	−2.45	0.76
Deep-Wet	**−1.65**	**−2.97**	**−0.36**
Time	**−0.03**	**−0.04**	**−0.02**
Veg * Time	0.01	−0.01	0.03
No Veg * Time	**0.04**	**0.02**	**0.06**
Deep-Dry * Time	**0.01**	**0.00**	**0.03**
Deep-Wet * Time	**0.02**	**0.01**	**0.04**

Note. The Intercept represents the Shallow-Dry group and is in per mille; the Time variable is the rate of change in Shallow-Dry in per mille per day; group * Time interactions show the effect of each group on the seasonal change of Recoδ13C. Bold values indicate statistical significance. CI = confidence interval.

Improvement of five AICc points justified the retention of a variable (Pinheiro & Bates, 2000; Zuur et al., 2009).

All analyses were conducted in R using lm (R Core Team, 2015) and lme4 (Bates et al., 2015) functions and the MuMIn (Bartoń, 2018), gridExtra (Auguie, 2017), and ggplot2 packages (Wickham, 2009).

3. Results

3.1. Seasonal Thaw, Water Table, and NDVI

Seasonal soil temperatures at 10-cm depth were similar between groups, increasing from May to July and decreasing from August to September (Figure 2a). The seasonal thaw, WTD, and NDVI dynamics were distinct between groups. Initial thaw of the top 25 cm was similar among all groups (Figure 2b). Once the first 25 cm thawed, thaw in Shallow-Dry, Veg, and No Veg groups increased gradually and linearly until the end of the season. In contrast, thaw depth in Deep-Dry and Deep-Wet increased sharply before continuing to increase more gradually. This abrupt increase in thaw depth indicates the presence of unfrozen soil layers that persisted through the winter. The large thaw increase in Deep-Dry and Deep-Wet also coincided with rising soil temperatures at 20 and 40 cm, indicating that surface thaw had allowed heat to penetrate the soil column (Figure S15). From July onward, thaw remained greater in Deep-Dry and Deep-Wet compared to Shallow-Dry, Veg, and No Veg (Text S3 and Table S2).

Water table dynamics over the season reflect the moisture conditions of the groups. In Shallow-Dry and Deep-Dry, WTD was on average 10 to 25 cm below the soil surface and at least 5 cm below the surface all season (Figures 2c and S1). In contrast, mean WTD in Deep-Wet was close to 0 cm (at the soil surface) and was high through the whole season fluctuating between saturated (−5 to 0 cm) or submerged (>0 cm; Figure 2c). WTD was not measured at Veg/No Veg plots. Based on weekly observations and landscape position, all Veg plots had water table below the surface. Some No Veg periodically had water at the soil surface (two of five plots), while others were drained all summer (three of five plots).

Seasonal NDVI showed that vegetation greenness was initially low, peaked in mid-July and decreased into September (Figure 2d). The patterns and magnitudes of NDVI were similar between Shallow-Dry, Deep-Dry, and Deep-Wet groups, while NDVI in the Veg group shows some delay in green-up and lower vegetation greenness all season. At CiPEHR, peak-season NDVI of Recoδ13C plots is within the NDVI range of the adjacent plots photographed all season (Figure 2d, "x" symbol).

3.2. Seasonal Reco Flux Rates

Ecosystem respiration had a strong seasonal pattern across all groups. At the beginning of the summer, Reco was low, increased significantly in late May, peaked in June and July, and declined to the lowest rates in September (Figures 3a–3e and Table 1). The seasonal pattern of Reco followed surface soil temperature (T_{5cm} and T_{10cm}; Figures 2a and S15) and the seasonal trend in NDVI (Figure 2d). Complete vegetation removal resulted in a 50–70% reduction in Reco throughout the season (No Veg: −63%, CI: −74 to −47; Figure 3c and Table 1). Among groups with similar thaw conditions, Shallow-Dry and Veg, there was no significant difference in the magnitude of Reco; however, there was a trend of lower Reco in Veg than in Shallow-Dry which could be related to the lower NDVI in Veg compared to Shallow-Dry (Figures 2d and 3a–3c and Table 1). Large differences in WTD conditions did not significantly change Reco flux rates (Figures 3d and 3e and Table 1).

3.3. Seasonal Recoδ^{13}C

The seasonal pattern of Recoδ^{13}C differed between thaw, moisture, and vegetation groups and, in conjunction with Reco flux rates, can inform shifting source contributions to Reco. At the beginning of the season, Recoδ^{13}C was the highest in Shallow-Dry with no significant difference in Veg or Deep-Dry (Intercept; Shallow-Dry: −22.54‰; Figures 3f, 3g, and 3i and Table 2). In contrast, Deep-Wet and No Veg had significantly lower Recoδ^{13}C than Shallow-Dry at the beginning of the season (Deep-Wet: −1.65‰, CI: −2.97 to −0.36; No Veg: −2.74‰, CI: −4.25 to −1.28; Figures 3h and 3j and Table 2).

Over the course of the summer, Recoδ^{13}C declined significantly in Shallow-Dry (Time: −0.03‰/day, CI: −0.04 to −0.03) with a similar slope in Veg (Figures 3f and 3g and Table 2). In Deep-Dry, the seasonal Recoδ^{13}C also declined but with a marginally less negative slope than Shallow-Dry (Deep-Dry * Time: 0.01‰/day, CI: 0.00 to 0.03; Figure 3i and Table 2). In No Veg, seasonal Recoδ^{13}C increased, and the slope was significantly higher than Shallow-Dry (No Veg * Time: 0.04, CI: 0.02 to 0.06; Figure 3h and Table 2). In Deep-Wet, seasonal Recoδ^{13}C remained constant with a significantly more positive slope than Shallow-Dry resulting in an overall 0 slope (Deep-Wet * Time: 0.02‰/day, CI: 0.01 to 0.04; Figure 3j and Table 2).

At the end of the season, the very last Recoδ^{13}C measurements in No Veg were filtered out due to extremely low flux rates (Text S1), so these two measurement dates were excluded from the entire seasonal trend analysis. In Shallow-Dry, Veg, Deep-Dry, and Deep-Wet, the end of season measurements continued along the same seasonal trajectories (Figures 3f–3j).

3.4. Peak Season Recoδ^{13}C in Thaw and Moisture Groups

At peak season, with three times as many plots as the seasonal sampling (see section 2.4.1), Recoδ^{13}C was higher in Deep-Dry than in Shallow-Dry and Deep-Wet (Figure 4). The group effects for peak season Recoδ^{13}C were not significant but were consistent with the seasonal trend of higher Recoδ^{13}C values in Deep-Dry compared to Shallow-Dry and Deep-Wet (Table 3).

4. Discussion

Disentangling the role of thaw and water dynamics on deep SOC loss is critical to understanding the vulnerability of permafrost SOC stocks to warming (Schuur et al., 2015). Previous work at CiPEHR and the EML Watershed has shown that newly thawed permafrost SOC is easily decomposable in the lab (Bracho et al., 2016; Salmon et al., 2018) and under field conditions, with only a 10-cm extension of ALT (Hicks Pries et al., 2013; Schuur et al., 2009). Since these initial studies, soil warming has deepened ALT up to 50 cm and doubled the amount of thawed SOC from 35 to 70 kg/cm^2 (Mauritz et al., 2017; Plaza et al., 2017). Using frequent seasonal Recoδ^{13}C measurements, we found partial support for our hypotheses that deep SOC loss increases with thaw and decreases with saturation. In the absence of vegetation, the positive Recoδ^{13}C slope indicates that deep SOC loss does increase with seasonal thaw (H1, Figure 1b). Under similar thaw conditions, the contribution of vegetation to Reco produced a negative seasonal Recoδ^{13}C slope and suggests that root respiration increases through the season. Contrary to expectation, much deeper ALT caused only a small increase in the seasonal Recoδ^{13}C slope (H2, Figure 1b). Given the observed patterns within No-Veg, Veg, and Shallow-Dry groups, the weak Recoδ^{13}C response in Deep-Dry likely reflects an increase in deep SOC as well as an increase in surface SOC, and root respiration that could mask deep SOC loss. In saturated areas, Recoδ^{13}C tended to be lower than in dry conditions which could be the result of either reduced deep SOC loss, altered diffusion, or fractionation from CH_4 cycling (H3, Figure 1b).

4.1. The Effects of Vegetation Removal on Seasonal Recoδ^{13}C

The seasonal trend in No-Veg establishes that deep SOC loss is detectable with seasonal Recoδ^{13}C measurements. In the complete absence of vegetation, Reco consists of only heterotrophic surface and deep SOC respiration, and we therefore expected the strongest signal from deep SOC respiration as seasonal thaw gradually exposes deeper soil layers (H1, Figure 1b). In No Veg, Recoδ^{13}C was low early in the growing season when the soil column was frozen, indicating a dominant contribution from surface SOC decomposition (Recoδ^{13}C: −23.5‰, Figures 1a and 3h). As thaw progressed through the growing season, increasing Recoδ^{13}C indicates progressively larger respiration contributions from deep SOC (Recoδ^{13}C: −21.5‰,
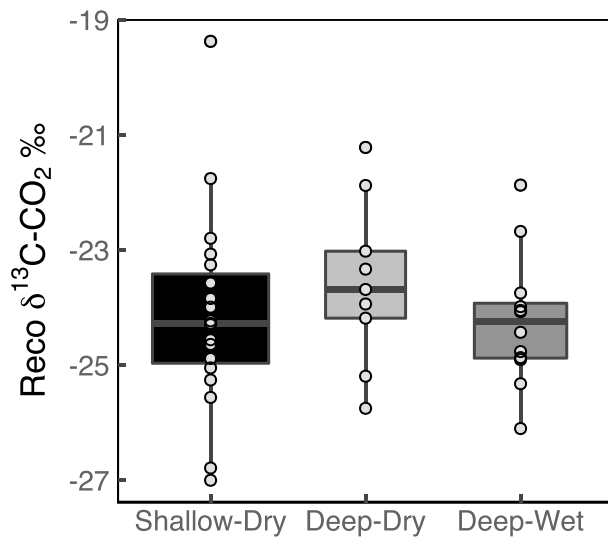
Figure 4. Peak season (9–11 July) Recoδ^{13}C (‰) for Shallow-Dry, Deep-Dry, and Deep-Wet groups at all Carbon in Permafrost Experimental Heating Research plots (total = 40) to capture greater sample size than for seasonal trends. Points represent individual plots within each group.

Figures 1a and 3h). The seasonal trend in No-Veg is therefore consistent with the prediction that Recoδ^{13}C would decline as the soil column thaws and deep SOC is decomposed.

4.2. Vegetation Contributions to Seasonal Recoδ^{13}C

Vegetation contributions to Recoδ^{13}C are evident when comparing the vegetated Shallow-Dry and Veg groups to No Veg because all three groups had similar thaw dynamics (Figure 2b). Respiration from aboveground vegetation and roots accounted for 30–60% of Reco (Figures 3a–3c and Table 2), similar to estimates at other tundra sites (McConnell et al., 2013; Segal & Sullivan, 2014). In Shallow-Dry and Veg, high early-season Recoδ^{13}C suggests that aboveground plant respiration (−22‰, Figures 1a and 3f–3h) dominates Reco as the vegetation begins to green. As the vegetation continues to green and surface soil warms, the declining Recoδ^{13}C trend most likely represents increasing root respiration (−25.5‰, Figure 1a) rather than surface SOC respiration (−23.5‰, Figure 1a) because No Veg also accounts for the negative isotopic signal from surface SOC decomposition. While the long-term exclusion of plant inputs could reduce surface SOC respiration in No Veg, surface soil decomposition in permafrost soil is generally not C limited (Pegoraro et al., 2018; Salmon et al., 2018; Wild et al., 2014). Thus, the difference between No Veg, Shallow-Dry, and Veg groups is more likely due to root respiration. The seasonal Recoδ^{13}C decline in the presence of vegetation is consistent with observations that leaf-greening precedes spring root growth (Kummerow & Russell, 1980; Shaver et al., 1986) and with tissue-specific estimates that root respiration exceeds shoot respiration in Moist Acidic Tundra during the growing season (Segal & Sullivan, 2014). It is interesting to note that as greenness declined at the end of the season (Figure 2d), Recoδ^{13}C also continued to decline, rather than increase as might be expected if deep SOC represents a larger portion of Reco once plants senesce. This continued seasonal Recoδ^{13}C decline supports observations that root activity extends beyond aboveground activity at the end of the growing season (Blume-Werry et al., 2016). Our results suggest that full interpretation of Reco dynamics requires a better understanding of root activity. Predictions of Arctic respiration that rely only on aboveground phenology or surface temperatures to predict ecosystem C exchange (Shaver et al., 2013) could miss important belowground contributions to Reco (Radville et al., 2016).

4.3. Deep Thaw Effects on Recoδ^{13}C

We expected that exposure of deep soil layers with experimental warming would increase Recoδ^{13}C, consistent with greater deep SOC loss (H2, Figure 1b). In Deep-Dry areas, as thaw depths diverged from Shallow-Dry, Recoδ^{13}C declined at a significantly lower rate than in Shallow-Dry areas (Figures 3f and 3i and Table 2). Similarly, Recoδ^{13}C from Deep-Dry plots tended to be higher than Shallow-Dry during peak-season sampling when triple the number of plots were sampled (Figure 4). Given that deep SOC losses were detectable when vegetation was removed, the weak effect of deepening ALT on Recoδ^{13}C suggests that soil warming also stimulates surface SOC decomposition and root respiration. The more negative δ^{13}C signatures of surface SOC and root respiration would counter the isotopic influence of deep SOC respiration and Recoδ^{13}C could thus remain unchanged (Figure 1a). This is consistent with another study at CiPEHR that found proportional deep SOC respiration declined during the first 2 years of warming (Hicks Pries et al., 2016). Lab incubations of CiPEHR soil suggest no initial warming effect on surface decomposition rates (Bracho et al., 2016). Changes in decomposition may be delayed as multiple ecosystem elements respond to warming, and microbial community shifts demonstrate that warming increases the capacity for more rapid SOC decomposition (Xue et al., 2016). Surface soil decomposition could increase after a longer period of warming and thaw, particularly if

Table 3
Peak Season (9–11 July) Recoδ13C Model Coefficients From a Comparison of 40 Carbon in Permafrost Experimental Heating Research Plots in Shallow-Dry, Deep-Dry, and Deep-Wet Groups

Response	Variable	Coefficients	2.5% CI	97.5% CI
Recoδ^{13}C (‰)	Intercept (Shallow-Dry)	−24.19	−24.89	−23.49
	Deep-Dry	0.54	−0.69	1.78
	Deep-Wet	−0.12	−1.24	1.01

Note. The model Intercept is the Shallow-Dry group, and coefficients are in per mille for Recoδ^{13}C. The Recoδ13C model $R^2 = -0.024$ and the ΔAICc = −3.66 (null–full model). CI = confidence interval.

limiting factors, like nitrogen (N) availability, increase (Mack et al., 2004; Salmon et al., 2018; Sistla et al., 2012; Wild et al., 2018). After 5 years of warming, in situ N-cycling rates in surface soils at CiPEHR had increased (Salmon et al., 2016), and plants can relocate additional N from the thawing permafrost front to surface soil (Keuper et al., 2017; Salmon et al., 2016). Thus, at this more advance stage of warming, increased surface SOC contributions to Reco are possible.

The N released from thawing permafrost also stimulates plant productivity (Keuper et al., 2012), and while increased aboveground biomass would cause Recoδ^{13}C to increase, root respiration contributes a more negative δ^{13}C signal. At CiPEHR, the first 5 years of warming stimulated a strong increase in plant growth, particularly of *Eriophorum vaginatum* (Salmon et al., 2016) which has higher relative root respiration rates than other Moist Acidic Tundra plant species (Segal & Sullivan, 2014) and could account for a larger proportion of respiration in deeply thawed areas. There is also some evidence that root density and root:shoot ratio increase with warming (Björk et al., 2007), which would lead to higher root contributions to Reco. In general, the response of roots to warming is mixed, with some studies also reporting decreased root growth (Wang et al., 2016) or no response to warming (Radville et al., 2016). Root dynamics are generally understudied in tundra systems (Iversen et al., 2014), and if warming responses are species or site specific, then root dynamics need to be quantified at individual sites to fully understand shifting Reco dynamics. Increased autotrophic respiration (Hicks Pries et al., 2015) and surface SOC turnover (Ziegler et al., 2017) with warming have been shown at other tundra and boreal sites contributing to the challenge of detecting deep SOC loss from surface Reco flux measurements alone. Additional insight could be gained from soil profile measurements and manipulations that isolate component fluxes such as vegetation removal, selective root exclusion, or separating surface soil decomposition.

4.4. Moisture Effects on Recoδ^{13}C

The effect of increasing soil moisture with permafrost thaw was of particular interest in this study because thawing soils are expected to become wetter before they become drier (Lawrence et al., 2015; Watts et al., 2014). We hypothesized that Recoδ^{13}C would be more negative under wet conditions due to suppressed deep SOC decomposition (H3, Figure 1b). The overall lower Recoδ^{13}C in Deep-Wet suggests a change in source contributions consistent with the expectation of lower deep SOC contributions. Lower Recoδ^{13}C could however also be explained by two alternate mechanisms: dynamic fractionation or methanogenesis effects on Recoδ^{13}C. Isotopic Reco measurements at the soil surface are influenced by physical soil diffusion properties (Cerling et al., 1991; Midwood & Millard, 2011). Under wet conditions, dynamic fractionation of upward diffusing CO_2 can cause Recoδ^{13}C to decline 3–4‰ compared to dry soil if chambers violate steady-state assumptions (Nickerson & Risk, 2009a; Phillips et al., 2010). Dynamic fractionation biases are thought to decrease in larger chambers and in chambers of our dimensions dynamic fractionation should cause Recoδ^{13}C to decline by only 1‰ (Ohlsson, 2009). Under field conditions, depth of collar insertion could matter more than dynamic fractionation, and Recoδ^{13}C is thought to equilibrate with soil $\delta^{13}CO_2$ at the depth of collar insertion (Kayler et al., 2008; Nickerson & Risk, 2009c; Snell et al., 2014). Here collars were installed at 6–7-cm depth and lower Recoδ^{13}C from Deep-Wet areas that reflects lower soil $\delta^{13}C$ in the soil column would be consistent with a change in respiration sources and potentially lower deep SOC loss.

The interpretation of Recoδ^{13}C from dry plots assumes that decomposition is primarily aerobic and does not account for the effects of methane (CH_4) production (methanogenesis) on $\delta^{13}CO_2$ (Treat et al., 2015; Whiticar, 1999; Zona et al., 2009). Under wet and saturated soil conditions, methanogenesis can cause $\delta^{13}CO_2$ within the soil column to increase up to 5‰ due to preferential $^{12}CO_2$ metabolism by methanogens (Knorr et al., 2008). In the opposite process, methane consumption (methanotrophy) causes Recoδ^{13}C to decline because the $\delta^{13}CO_2$ respired from CH_4 substrates is very negative (Whiticar, 1999). At CiPEHR, landscape-level CH_4 flux increases with seasonal thaw which indicates increasing methanotrophy throughout the season (Taylor et al., 2018) and net CH_4 flux from wetter areas accounts for less than 1% of annual Reco (CO_2 flux; Natali et al., 2015). Despite the small budget component of net CH_4 flux, dominant methanotrophy early in the season and progressively increasing methanogenesis could explain the Recoδ^{13}C patterns in Deep-Wet areas. If the net CH_4 flux at CiPEHR is equal to CH_4 production, then 1% of the CO_2 released via Reco would be affected by methanogenic fractionation. Assuming that methanogenesis occurs via hydrogenotrophy which has the strongest fractionation effect, Recoδ^{13}C would thus increase by 1‰. On

the other hand, if 1% of Reco is affected by methanotrophy with $\delta^{13}CH_4$ substrates as low as $-110‰$, then Recoδ^{13}C could decrease by 1‰ (Knorr et al., 2008; Whiticar, 1999). Early in the season, Recoδ^{13}C was 1.65‰ lower in Deep-Wet compared to Shallow-Dry and Deep-Dry areas (Figures 3f, 3i, and 3j), consistent with methanotrophy early in the season. The steeper Recoδ^{13}C slope in Deep-Wet would be consistent with greater methanogenesis as the soil thaws. And the overall more negative Recoδ^{13}C in Deep-Wet areas implies that methanotrophy keeps net CH_4 fluxes low (Kettunen et al., 1999). Altered Recoδ^{13}C under wet conditions could therefore result from CH_4 contributions without any change in shoot, root, shallow, or deep SOC respiration. Our interpretations of Recoδ^{13}C are based on SOC δ^{13}C respiration in aerobic incubations and might be improved by also considering anaerobic $\delta^{13}CO_2$ end-members. Coupling field measurements of Recoδ^{13}C with more detailed CH_4 flux and δ^{13}C, CO_2, and CH_4 soil profiles would help to further elucidate how variation in CO_2 and CH_4 production affects δ^{13}C signatures and provide further insight to deep SOC vulnerability to thaw.

5. Conclusions

Permafrost systems in the Arctic are predicted to experience warmer temperatures, increasing precipitation, and accelerated permafrost thaw (Bintanja & Andry, 2017; IPCC, 2013; Westermann et al., 2011). Warming in the next century could cause permafrost systems to initially become wetter and then drier, despite increased precipitation, due to surface subsidence followed by widespread landscape drainage (Lawrence et al., 2015). Predictions of permafrost C loss should therefore consider the effects of both wet and dry conditions on deep SOC vulnerability (Schuur et al., 2015). Here seasonal Recoδ^{13}C measurements indicate that thaw and moisture conditions alter Reco sources, even when Reco flux rates remain similar. In the prevailingly shallow-thawed and dry soil conditions of the study area, Reco appears to be dominated by surface soil decomposition and autotrophic root respiration. Yet, when the vegetation signal was removed, there was evidence of increasing deep SOC contributions to Reco which means deep SOC losses could be underestimated in surface flux measurements. Deep thaw and dry conditions tended to have higher Recoδ^{13}C signatures as the season progressed, consistent with greater contributions from deep soil respiration. Increased moisture changed Recoδ^{13}C and suggests altered CO_2 production pathways either due to reduced deep SOC loss, changes in soil diffusivity, or a shift in CH_4 production and consumption. The development of portable instruments for δ^{13}C measurements has increased the speed, ease, and cost effectiveness with which Recoδ^{13}C can be measured (Midwood & Millard, 2011). With weekly Recoδ^{13}C, it was possible to interpret shifting Reco sources in the context of thaw, surface soil temperatures, and aboveground plant dynamics. However, the small seasonal changes in Recoδ^{13}C and the dominant signal from autotrophic and surface soil respiration made it difficult to detect deep SOC contributions with surface flux measurements alone. Future studies that simultaneously quantify root and shoot respiration dynamics, CH_4 flux, soil δ^{13}C profiles, or pair δ^{13}C with strategic Δ^{14}C sampling, could further elucidate changes in Reco source contributions.

References

Abbott, B. W., Jones, J., Schuur, E. A. G., Chapin, F. S. III, Bowden, W., Bret-Harte, M., Epstein, H., et al. (2016). Biomass offsets little or none of permafrost carbon release from soils, streams, and wildfire: An expert assessment. *Environmental Research Letters*, *11*(3), 034014. https://doi.org/10.1088/1748-9326/11/3/034014

Auguie, B. (2017). gridExtra: Miscellaneous functions for "Grid" graphics.

Bartoń, K. (2018). MuMIn: Multi-Model Inference.

Bates, D., Maechler, M., Bolker, B., & Walker, S. (2015). Fitting linear mixed-effects models using lme4. *Journal of Statistical Software*, *67*, 1–48.

Belshe, E. F., Schuur, E. A. G., & Bolker, B. M. (2013). Tundra ecosystems observed to be CO_2 sources due to differential amplification of the carbon cycle. *Ecology Letters*, *16*(10), 1307–1315. https://doi.org/10.1111/ele.12164

Bintanja, R., & Andry, O. (2017). Towards a rain-dominated Arctic. *Nature Climate Change*, *7*(4), 263–267. https://doi.org/10.1038/nclimate3240

Björk, R. G., Majdi, H., Klemedtsson, L., Lewis-jonsson, L., Molau, U., & Björk, R. G. (2007). Long-term warming effects on root morphology, root mass distribution, and microbial activity in two dry tundra plant communities in northern Sweden. *New Phytologist*, *176*(4), 862–873. https://doi.org/10.1111/j.1469-8137.2007.02231.x

Blume-Werry, G., Wilson, S. D., Kreyling, J., & Milbau, A. (2016). The hidden season: Growing season is 50% longer below than above ground along an arctic elevation gradient. *New Phytologist*, *209*(3), 978–986. https://doi.org/10.1111/nph.13655

Bowling, D. R., Pataki, D. E., & Randerson, J. T. (2008). Carbon isotopes in terrestrial ecosystem pools and CO_2 fluxes. *New Phytologist*, *178*(1), 24–40. https://doi.org/10.1111/j.1469-8137.2007.02342.x

Bracho, R., Natali, S., Pegoraro, E., Crummer, K. G., Schädel, C., Celis, G., Hale, L., et al. (2016). Temperature sensitivity of organic matter decomposition of permafrost-region soils during laboratory incubations. *Soil Biology and Biochemistry*, *97*, 1–14. https://doi.org/10.1016/j.soilbio.2016.02.008

Carey, J. C., Tang, J., Templer, P. H., Kroeger, K. D., Crowther, T. W., Burton, A. J., Dukes, J. S., et al. (2016). Temperature response of soil respiration largely unaltered with experimental warming. *Proceedings of the National Academy of Sciences*, *113*(48), 13,797–13,802. https://doi.org/10.1073/pnas.1605365113

Cerling, T. E., Solomon, D. K., Quade, J., & Bowman, J. R. (1991). On the isotopic composition of carbon in soil carbon dioxide. *Geochimica et Cosmochimica Acta*, *55*(11), 3403–3405. https://doi.org/10.1016/0016-7037(91)90498-T

R Core Team (2015). R: A language and environment for statistical computing. R Foundation for Statistical Computing, Vienna, Austria.

Deane-Coe, K. K., Mauritz, M., Celis, G., Salmon, V., Crummer, K. G., Natali, S. M., & Schuur, E. A. G. (2015). Experimental warming alters productivity and isotopic signatures of tundra mosses. *Ecosystems*, *18*(6), 1070–1082. https://doi.org/10.1007/s10021-015-9884-7

Dorrepaal, E., Toet, S., Van Logtestijn, R. S. P., Swart, E., Van De Weg, M. J., Callaghan, T. V., & Aerts, R. (2009). Carbon respiration from subsurface peat accelerated by climate warming in the subarctic. *Nature*, *460*(7255), 616–619. https://doi.org/10.1038/nature08216

Ebert, C. H., Schuur, E. A. G., & Hicks-Pries, C. E. (2016). Eight Mile Lake Research Watershed, thaw gradient, the radiocarbon value of ecosystem respiration, 2004–2016 III: Atm. Bonanza Creek, LTER - University of Alaska Fairbanks.

Ehleringer, J. (2000). Carbon isotope ratios in belowground carbon cycle processes. *Ecological Applications*, *10*(2), 412–422. https://doi.org/10.1890/1051-0761(2000)010[0412:CIRIBC]2.0.CO;2

Elberling, B., Michelsen, A., Schädel, C., Schuur, E. A. G., Christiansen, H. H., Berg, L., Tamstorf, M. P., et al. (2013). Long-term CO_2 production following permafrost thaw. *Nature Climate Change*, *3*(10), 890–894. https://doi.org/10.1038/nclimate1955

Esmeijer-Liu, A. J., Kürschner, W. M., Lotter, A. F., Verhoeven, J. T. A., & Goslar, T. (2012). Stable carbon and nitrogen isotopes in a peat profile are influenced by early stage diagenesis and changes in atmospheric CO_2 and N deposition. *Water, Air, & Soil Pollution*, *223*, 2007–2022.

Graven, H., Xu, X., Guilderson, T. P., Keeling, R. F., Trumbore, S. E., & Tyler, S. (2013). Comparison of independent $\Delta^{14}CO_2$ records at Point Barrow, Alaska. *Radiocarbon*, *55*(03), 1541–1545. https://doi.org/10.1017/S0033822200048463

Harden, J. W., Koven, C. D., Ping, C.-L., Hugelius, G., David McGuire, A., Camill, P., Jorgenson, T., et al. (2012). Field information links permafrost carbon to physical vulnerabilities of thawing. *Geophysical Research Letters*, *39*, L15704. https://doi.org/10.1029/2012GL051958

Hicks Pries, C. E., Logtestijn, R. S. P., Schuur, E. A. G., Natali, S. M., Cornelissen, J. H. C., Aerts, R., & Dorrepaal, E. (2015). Decadal warming causes a consistent and persistent shift from heterotrophic to autotrophic respiration in contrasting permafrost ecosystems. *Global Change Biology*, *21*(12), 4508–4519. https://doi.org/10.1111/gcb.13032

Hicks Pries, C. E., Schuur, E. A. G., & Crummer, K. G. (2013). Thawing permafrost increases old soil and autotrophic respiration in tundra: Partitioning ecosystem respiration using $\delta^{13}C$ and $\Delta^{14}C$. *Global Change Biology*, *19*(2), 649–661. https://doi.org/10.1111/gcb.12058

Hicks Pries, C. E., Schuur, E. A. G., & Crummer, K. G. (2012). Holocene carbon stocks and carbon accumulation rates altered in soils undergoing permafrost thaw. *Ecosystems*, *15*(1), 162–173. https://doi.org/10.1007/s10021-011-9500-4

Hicks Pries, C. E., Schuur, E. A. G., Natali, S. M., & Crummer, K. G. (2016). Old soil carbon losses increase with ecosystem respiration in experimentally thawed tundra. *Nature Climate Change*, *6*(2), 214–218. https://doi.org/10.1038/nclimate2830

Hugelius, G., Strauss, J., Zubrzycki, S., Harden, J. W., Schuur, E. A. G., Ping, C.-L., Schirrmeister, L., et al. (2014). Estimated stocks of circumpolar permafrost carbon with quantified uncertainty ranges and identified data gaps. *Biogeosciences*, *11*(23), 6573–6593. https://doi.org/10.5194/bg-11-6573-2014

IPCC (2013). In T. F. Stocker, D. Qin, G.-K. Plattner, M. Tignor, S. K. Allen, J. Boschung, et al. (Eds.), *Climate change 2013: The physical science basis. Contribution of Working Group I to the Fifth Assessment Report of the Intergovernmental Panel on Climate Change.* Cambridge, UK and New York: Cambridge University Press.

Iversen, C. M., Sloan, V. L., Sullivan, P. F., Euskirchen, E. S., Mcguire, A. D., Norby, R. J., et al. (2014). Tansley review The unseen iceberg: Plant roots in Arctic tundra.

Jorgenson, T. M., Harden, J., Kanevskiy, M., O'Donnell, J., Wickland, K., Ewing, S., Manies, K., et al. (2013). Reorganization of vegetation, hydrology and soil carbon after permafrost degradation across heterogeneous boreal landscapes. *Environmental Research Letters*, *8*, 3.

Kayler, Z. E., Sulzman, E. W., Marshall, J. D., Mix, A., Rugh, W. D., & Bond, B. J. (2008). A laboratory comparison of two methods used to estimate the isotopic composition of soil $\delta^{13}CO_2$ efflux at steady state. *Rapid Communications in Mass Spectrometry*, *22*(16), 2533–2538. https://doi.org/10.1002/rcm.3643

Keeling, C. D. (1958). The concentration and isotopic abundances of atmospheric carbon dioxide in rural areas. *Geochimica et Cosmochimica Acta*, *13*(4), 322–334. https://doi.org/10.1016/0016-7037(58)90033-4

Keeling, C. D. (1961). The concentration and isotopic abundances of carbon dioxide in rural and marine air. *Geochimica et Cosmochimica Acta*, *24*(3–4), 277–298. https://doi.org/10.1016/0016-7037(61)90023-0

Kettunen, A., Kaitala, V., Lehtinen, A., Lohila, A., & Alm, J. (1999). Methane production and oxidation potentials in relation to water table fluctuations in two boreal mires. *Soil Biology and Biochemistry*, *31*(12), 1741–1749. https://doi.org/10.1016/S0038-0717(99)00093-0

Keuper, F., Dorrepaal, E., van Bodegom, P. M., van Logtestijn, R., Venhuizen, G., van Hal, J., & Aerts, R. (2017). Experimentally increased nutrient availability at the permafrost thaw front selectively enhances biomass production of deep-rooting subarctic peatland species. *Global Change Biology*, *23*(10), 4257–4266. https://doi.org/10.1111/gcb.13804

Keuper, F., van Bodegom, P. M., Dorrepaal, E., Weedon, J. T., van Hal, J., van Logtestijn, R. S. P., & Aerts, R. (2012). A frozen feast: Thawing permafrost increases plant-available nitrogen in subarctic peatlands. *Global Change Biology*, *18*(6), 1998–2007. https://doi.org/10.1111/j.1365-2486.2012.02663.x

Knorr, K.-H., Glaser, B., & Blodau, C. (2008). Fluxes and ^{13}C isotopic composition of dissolved carbon and pathways of methanogenesis in a fen soil exposed to experimental drought. *Biogeosciences Discussions*, *5*(2), 1319–1360. https://doi.org/10.5194/bgd-5-1319-2008

Kummerow, J., & Russell, M. (1980). Seasonal root growth in the Arctic tussock tundra. *Oecologia*, *47*(2), 196–199. https://doi.org/10.1007/BF00346820

Lawrence, D. M., Koven, C. D., Swenson, S. C., Riley, W. J., & Slater, A. G. (2015). Permafrost thaw and resulting soil moisture changes regulate projected high-latitude CO_2 and CH_4 emissions. *Environmental Research Letters*, *10*(9), 94011. https://doi.org/10.1088/1748-9326/10/9/094011

Lee, H., Schuur, E. A. G., & Vogel, J. G. (2010). Soil CO_2 production in upland tundra where permafrost is thawing. *Journal of Geophysical Research*, *115*, G01009. https://doi.org/10.1029/2008JG000906

Liljedahl, A. K., Boike, J., Daanen, R. P., Fedorov, A. N., Frost, G. V., Grosse, G., Hinzman, L. D., et al. (2016). Pan-Arctic ice-wedge degradation in warming permafrost and its influence on tundra hydrology. *Nature Geoscience*, *9*(4), 312–318. https://doi.org/10.1038/ngeo2674

Lloyd, J., & Taylor, J. A. (1994). On the temperature-dependence of soil respiration. *Functional Ecology*, *8*(3), 315–323. https://doi.org/10.2307/2389824

Mack, M. C., Schuur, E. A. G., Bret-Harte, M. S., Shaver, G. R., & Chapin, F. S. (2004). Ecosystem carbon storage in Arctic tundra reduced by long-term nutrient fertilization. *Nature*, *431*(7007), 440–443. https://doi.org/10.1038/nature02887

Mahecha, M. D., Reichstein, M., Carvalhais, N., Lasslop, G., Lange, H., Seneviratne, S. I., Vargas, R., et al. (2010). Global convergence in the temperature sensitivity of respiration at ecosystem level. *Science*, *329*(5993), 838–840. https://doi.org/10.1126/science.1189587

Mauritz, M., Bracho, R., Celis, G., Hutchings, J., Natali, S. M., Pegoraro, E., Salmon, V. G., et al. (2017). Nonlinear CO_2 flux response to 7 years of experimentally induced permafrost thaw. *Global Change Biology*, *23*(9), 3646–3666. https://doi.org/10.1111/gcb.13661

Mauritz, M., & Schuur, E. A. G. (2018). Eight mile Lake research watershed, carbon in permafrost experimental heating and drying research (CiPEHR and DryPEHR): Weekly 13C Keeling plot signatures of ecosystem respiration from CiPEHR, DryPEHR and vegetation removal plots, and auxilliary data, 201. Bonanza Creek LTER - University of Alaska Fairbanks BNZ: 700.

McConnell, N. A., Turetsky, M. R., David McGuire, A., Kane, E. S., Waldrop, M. P., & Harden, J. W. (2013). Controls on ecosystem and root respiration across a permafrost and wetland gradient in interior Alaska. *Environmental Research Letters*, *8*(4), 045029. https://doi.org/10.1088/1748-9326/8/4/045029

Midwood, A. J., & Millard, P. (2011). Challenges in measuring the $\delta^{13}C$ of the soil surface CO_2 efflux. *Rapid Communications in Mass Spectrometry*, *25*(1), 232–242.

Natali, S. M., Schuur, E. A. G., Mauritz, M., Schade, J. D., Celis, G., Crummer, K. G., Johnston, C., et al. (2015). Permafrost thaw and soil moisture driving CO_2 and CH_4 release from upland tundra. *Journal of Geophysical Research: Biogeosciences*, *120*, 525–537. https://doi.org/10.1002/2014JG002872

Natali, S. M., Schuur, E. A. G., & Rubin, R. L. (2012). Increased plant productivity in Alaskan tundra as a result of experimental warming of soil and permafrost. *Journal of Ecology*, *100*(2), 488–498. https://doi.org/10.1111/j.1365-2745.2011.01925.x

Natali, S. M., Schuur, E. A. G., Trucco, C., Hicks Pries, C. E., Crummer, K. G., & Baron Lopez, A. F. (2011). Effects of experimental warming of air, soil and permafrost on carbon balance in Alaskan tundra. *Global Change Biology*, *17*(3), 1394–1407. https://doi.org/10.1111/j.1365-2486.2010.02303.x

Natali, S. M., Schuur, E. A. G., Webb, E. E., Pries, C. E. H., & Crummer, K. G. (2014). Permafrost degradation stimulates carbon loss from experimentally warmed tundra. *Ecology*, *95*(3), 602–608. https://doi.org/10.1890/13-0602.1

Newman, S., Xu, X., Gurney, K. R., Hsu, Y. K., Li, K. F., Jiang, X., Keeling, R., et al. (2016). Toward consistency between trends in bottom-up CO_2 emissions and top-down atmospheric measurements in the Los Angeles megacity. *Atmospheric Chemistry and Physics*, *16*(6), 3843–3863. https://doi.org/10.5194/acp-16-3843-2016

Nickerson, N., & Risk, D. (2009a). A numerical evaluation of chamber methodologies used in measuring the $\delta^{13}C$ of soil respiration. *Rapid Communications in Mass Spectrometry*, *23*(17), 2802–2810. https://doi.org/10.1002/rcm.4189

Nickerson, N., & Risk, D. (2009b). Keeling plots are non-linear in non-steady state diffusive environments. *Geophysical Research Letters*, *36*, L08401. https://doi.org/10.1029/2008GL036945

Nickerson, N., & Risk, D. (2009c). Physical controls on the isotopic composition of soil-respired CO_2. *Journal of Geophysical Research*, *114*, G02028. https://doi.org/10.1029/2008JG000766

Nowinski, N. S., Taneva, L., Trumbore, S. E., & Welker, J. M. (2010). Decomposition of old organic matter as a result of deeper active layers in a snow depth manipulation experiment. *Oecologia*, *163*(3), 785–792. https://doi.org/10.1007/s00442-009-1556-x

O'Donnell, J. A., Jorgenson, M. T., Harden, J. W., McGuire, A. D., Kanevskiy, M. Z., & Wickland, K. P. (2012). The effects of permafrost thaw on soil hydrologic, thermal and carbon dynamics in an Alaskan peatland. *Ecosystems*, *15*(2), 213–229. https://doi.org/10.1007/s10021-011-9504-0

Ohlsson, K. E. A. (2009). Reduction of bias in static closed chamber measurement of $\delta^{13}C$ in soil CO_2 efflux. *Rapid Communications in Mass Spectrometry*, *24*, 180–184.

Olefeldt, D., Turetsky, M., Crill, P., & A, M. D. (2013). Environmental and physical controls on northern terrestrial methane emissions across permafrost zones. *Global Change Biology*, *19*(2), 589–603. https://doi.org/10.1111/gcb.12071

Osterkamp, T. E., Jorgenson, M. T., Schuur, E. A. G., Shur, Y. L., Kanevskiy, M. Z., Vogel, J. G., & Tumskoy, V. E. (2009). Physical and ecological changes associated with warming permafrost and thermokarst in interior Alaska. *Permafrost and Periglacial Processes*, *20*(3), 235–256. https://doi.org/10.1002/ppp.656

Pataki, D. E., Ehleringer, J. R., Flanagan, L. B., Yakir, D., Bowling, D. R., Still, C. J., Buchmann, N., et al. (2003). The application and interpretation of Keeling plots in terrestrial carbon cycle research. *Global Biogeochemical Cycles*, *17*(1), 1022. https://doi.org/10.1029/2001GB001850

Pegoraro, E., Mauritz, M., Bracho, R., Ebert, C., Dijkstra, P., Hungate, B. A., Konstantinidis, K. T., et al. (2018). Glucose addition increases the magnitude and decreases the age of soil respired carbon in a long-term permafrost incubation study. *Soil Biology and Biochemistry*. https://doi.org/10.1016/j.soilbio.2018.10.009

Phillips, C. L., Nickerson, N., Risk, D., Kayler, Z. E., Andersen, C., Mix, A., & Bond, B. J. (2010). Soil moisture effects on the carbon isotope composition of soil respiration. *Rapid Communications in Mass Spectrometry*, *24*(9), 1271–1280. https://doi.org/10.1002/rcm.4511

Ping, C. L., Jastrow, J. D., Jorgenson, M. T., Michaelson, G. J., & Shur, Y. L. (2015). Permafrost soils and carbon cycling. *The Soil*, *1*(1), 147–171. https://doi.org/10.5194/soil-1-147-2015

Pinheiro, J. C., & Bates, D. M. (2000). Extending the basic linear mixed-effects model. In *Mixed-effects models in S and S-PLUS* (pp. 201–270). New York: Springer-Verlag.

Plaza, C., Schuur, E. A. G., & Pegoraro, E. F. (2017). Eight Mile Lake Research Watershed, Carbon in Permafrost Experimental Heating Research (CiPEHR): Physical and chemical properties of soils, 2009-2013. Bonanza Creek, LTER - University of Alaska Fairbanks BNZ: 655.

Radville, L., Post, E., & Eissenstat, D. M. (2016). Root phenology in an Arctic shrub-graminoid community: The effects of long-term warming and herbivore exclusion. *Climate Change Responses*, *3*(1), 4. https://doi.org/10.1186/s40665-016-0017-0

Salmon, V. G., Schädel, C., Bracho, R., Pegoraro, E., Celis, G., Mauritz, M., Mack, M. C., et al. (2018). Adding depth to our understanding of nitrogen dynamics in permafrost soils. *Journal of Geophysical Research: Biogeosciences*, *123*, 2497–2512. https://doi.org/10.1029/2018JG004518

Salmon, V. G., Soucy, P., Mauritz, M., Celis, G., Natali, S. M., Mack, M. C., & Schuur, E. A. G. (2016). Nitrogen availability increases in a tundra ecosystem during five years of experimental permafrost thaw. *Global Change Biology*, *22*(5), 1927–1941. https://doi.org/10.1111/gcb.13204

Schädel, C., Bader, M. K. F., Schuur, E. A. G., Biasi, C., Bracho, R., Capek, P., De Baets, S., et al. (2016). Potential carbon emissions dominated by carbon dioxide from thawed permafrost soils. *Nature Climate Change Change*, *6*(10), 950–953. https://doi.org/10.1038/nclimate3054

Schädel, C., Schuur, E. A. G., Bracho, R., Elberling, B., Knoblauch, C., Lee, H., Luo, Y., et al. (2014). Circumpolar assessment of permafrost C quality and its vulnerability over time using long-term incubation data. *Global Change Biology*, *20*(2), 641–652. https://doi.org/10.1111/gcb.12417

Schuur, E. A. G., Crummer, K. G., Vogel, J. G., & Mack, M. C. (2007). Plant species composition and productivity following permafrost thaw and thermokarst in Alaskan tundra. *Ecosystems*, *10*(2), 280–292. https://doi.org/10.1007/s10021-007-9024-0

Schuur, E. A. G., McGuire, A. D., Schädel, C., Grosse, G., Harden, J. W., Hayes, D. J., Hugelius, G., et al. (2015). Climate change and the permafrost carbon feedback. *Nature*, *520*(7546), 171–179. https://doi.org/10.1038/nature14338

Schuur, E. A. G., Trumbore, S. E., Mack, M. C., & Harden, J. W. (2003). Isotopic composition of carbon dioxide from a boreal forest fire: Inferring carbon loss from measurements and modeling. *Global Biogeochemical Cycles*, *17*(1), 1001. https://doi.org/10.1029/2001GB001840

Schuur, E. A. G., Vogel, J. G., Crummer, K. G., Lee, H., Sickman, J. O., & Osterkamp, T. E. (2009). The effect of permafrost thaw on old carbon release and net carbon exchange from tundra. *Nature*, *459*(7246), 556–559. https://doi.org/10.1038/nature08031

Segal, A. D., & Sullivan, P. F. (2014). Identifying the sources and uncertainties of ecosystem respiration in Arctic tussock tundra. *Biogeochemistry*, *121*(3), 489–503. https://doi.org/10.1007/s10533-014-0017-8

Shaver, G. R., Chappin, F. III, & Gartnert, B. L. (1986). Factors limiting seasonal growth and peak biomass accumulation in Eriophorum vaginatum in Alaskan tussock tundra author (s): G. R. Shaver, F. Chapin III and Barbara L. Gartner published by: British Ecological Society stable URL: http://www.jstor. *Journal of Ecology*, *74*(1), 257–278. https://doi.org/10.2307/2260362

Shaver, G. R., Rastetter, E. B., Salmon, V., Street, L. E., van de Weg, M. J., Rocha, A., van Wijk, M. T., et al. (2013). Pan-Arctic modelling of net ecosystem exchange of CO_2. *Philosophical Transactions of the Royal Society, B: Biological Sciences*, 368. https://doi.org/10.1098/rstb.2012.0485

Sistla, S. A., Asao, S., & Schimel, J. P. (2012). Detecting microbial N-limitation in tussock tundra soil: Implications for Arctic soil organic carbon cycling. *Soil Biology and Biochemistry*, *55*, 78–84. https://doi.org/10.1016/j.soilbio.2012.06.010

Snell, H. S. K., Robinson, D., & Midwood, A. J. (2014). Minimising methodological biases to improve the accuracy of partitioning soil respiration using natural abundance ^{13}C. *Rapid Communications in Mass Spectrometry*, *28*(21), 2341–2351. https://doi.org/10.1002/rcm.7017

Taylor, M. A., Celis, G., Ledman, J. D., Bracho, R., & Schuur, E. A. G. (2018). Methane efflux measured by eddy covariance in Alaskan upland tundra undergoing permafrost degradation. *Journal of Geophysical Research: Biogeosciences*, *23*, 1–16. https://doi.org/10.1029/2018JG004444

Treat, C. C., Natali, S. M., Ernakovich, J., Iversen, C. M., Lupascu, M., McGuire, A. D., Norby, R. J., et al. (2015). A pan-Arctic synthesis of CH_4 and CO_2 production from anoxic soil incubations. *Global Change Biology*, *21*(7), 2787–2803. https://doi.org/10.1111/gcb.12875

Vogel, J., Schuur, E. A. G., Trucco, C., & Lee, H. (2009). Response of CO_2 exchange in a tussock tundra ecosystem to permafrost thaw and thermokarst development. *Journal of Geophysical Research*, *114*, G04018. https://doi.org/10.1029/2008JG000901

Walker, M. D., Walker, D. A., Welker, J. M., Arft, A. M., Bardsley, T., Brooks, P. D., Fahnestock, J. T., et al. (1999). Long-term experimental manipulation of winter snow regime and summer temperature in arctic and alpine tundra. *Hydrological Processes*, *13*(14–15), 2315–2330. https://doi.org/10.1002/(SICI)1099-1085(199910)13:14/15<2315::AID-HYP888>3.0.CO;2-A

Wang, P., Heijmans, M. M. P. D., Mommer, L., van Ruijven, J., Maximov, T. C., & Berendse, F. (2016). Belowground plant biomass allocation in tundra ecosystems and its relationship with temperature. *Environmental Research Letters*, *11*(5), 055003. https://doi.org/10.1088/1748-9326/11/5/055003

Watts, J. D., Kimball, J. S., Parmentier, F. J. W., Sachs, T., Rinne, J., Zona, D., Oechel, W., et al. (2014). A satellite data driven biophysical modeling approach for estimating northern peatland and tundra CO_2 and CH_4 fluxes. *Biogeosciences*, *11*(7), 1961–1980. https://doi.org/10.5194/bg-11-1961-2014

Wehr, R., & Saleska, S. R. (2017). The long-solved problem of the best-fit straight line: Application to isotopic mixing lines. *Biogeosciences*, *14*(1), 17–29. https://doi.org/10.5194/bg-14-17-2017

Westermann, S., Boike, J., Langer, M., Schuler, T. V., & Etzelmüller, B. (2011). Modeling the impact of wintertime rain events on the thermal regime of permafrost. *The Cryosphere*, *5*(4), 945–959. https://doi.org/10.5194/tc-5-945-2011

Whiticar, M. J. (1999). Carbon and hydrogen isotope systematics of bacterial formation and oxidation of methane. *Chemical Geology*, *161*(1-3), 291–314. https://doi.org/10.1016/S0009-2541(99)00092-3

Wickham, H. (2009). *ggplot2: Elegant graphics for data analysis*. New York: Springer-Verlag. https://doi.org/10.1007/978-0-387-98141-3

Wild, B., Alves, R. J. E., Bárta, J., Čapek, P., Gentsch, N., Guggenberger, G., Hugelius, G., et al. (2018). Amino acid production exceeds plant nitrogen demand in Siberian tundra. *Environmental Research Letters*, *13*(3), 034002. https://doi.org/10.1088/1748-9326/aaa4fa

Wild, B., Schnecker, J., Alves, R. J. E., Barsukov, P., Barta, J., Capek, P., Gentsch, N., et al. (2014). Input of easily available organic C and N stimulates microbial decomposition of soil organic matter in arctic permafrost soil. *Soil Biology and Biochemistry*, *75*(100), 143–151. https://doi.org/10.1016/j.soilbio.2014.04.014

Xue, K., Yuan, M. M., Shi, Z. J., Qin, Y., Deng, Y., Cheng, L., Wu, L., et al. (2016). Tundra soil carbon is vulnerable to rapid microbial decomposition under climate warming. *Nature Climate Change*, *6*(6), 595–600. https://doi.org/10.1038/nclimate2940

Ziegler, S. E., Benner, R., Billings, S. A., Edwards, K. A., Philben, M., Zhu, X., & Laganière, J. (2017). Climate warming can accelerate carbon fluxes without changing soil carbon stocks. *Frontiers in Earth Science*, *5*, 2.

Zobitz, J. M., Keener, J. P., Schnyder, H., & Bowling, D. R. (2006). Sensitivity analysis and quantification of uncertainty for isotopic mixing relationships in carbon cycle research. *Agricultural and Forest Meteorology*, *136*(1–2), 56–75. https://doi.org/10.1016/j.agrformet.2006.01.003

Zona, D., Oechel, W. C., Kochendorfer, J., Paw, U. K. T., Salyuk, A. N., Olivas, P. C., Oberbauer, S. F., et al. (2009). Methane fluxes during the initiation of a large-scale water table manipulation experiment in the Alaskan Arctic tundra. *Global Biogeochemical Cycles*, *23*, GB2013. https://doi.org/10.1029/2009GB003487

Zuur, A. F., Ieno, E. N., Walker, N., Saveliev, A. A., & Smith, G. M. (2009). *Mixed effects models and extensions in ecology with R*. New York: Springer. https://doi.org/10.1007/978-0-387-87458-6